# Near-Threshold Propagation of Mode II and Mode III Cracks

**L. Holáň[1], R. Pippan[2], J. Pokluda[1], J. Horníková[1], A. Hohenwarter[2], K. Slámečka[1]**

[1] Brno University of Technology, Faculty of Mechanical Engineering, Technická 2, 616 69 Brno, Czech Republic, y101840@stud.fme.vutbr.cz
[2] Erich Schmid Institute of Material Science, Austrian Academy of Sciences, Jahnstrasse 12, 8700 Leoben, Austria

***ABSTRACT.*** *Two prototype experiments allowing a simultaneous mode II and mode III fatigue crack propagation in a single specimen are described and the differences in related to growth are discussed. The cylindrical specimens made of austenitic and ferritic steels with circumferential V-notch were prepared. The specially manufactured loading setups enabled to assure a pure remote shear mode II at both the top and the bottom sites of the specimen, whereas a pure mode III operated at front and back sites. Differences between the mechanisms of crack propagation were assessed by means of the 3D fractographical analysis based on the stereophotogrammetry in SEM. The stress intensity factors $K_{II}$ and $K_{III}$ were determined by a numerical method based on the ANSYS code and compared with asymptotically computed values of $K_{III}$. The threshold values $\Delta K_{IIth}$ (R = 0.1) were found to be of 1.2 MPam$^{1/2}$ in ferrite and of 3.5 MPam$^{1/2}$ in austenite, whereas $\Delta K_{IIIth} \approx 2.0$ .in ferrite and $\Delta K_{IIIth} \approx 4.7$ MPam$^{1/2}$ in austenite. In both steels, the near-threshold crack growth rate under the mode II was found to be much higher than that under the mode III.*

## INTRODUCTION

While the principal micromechanisms of fatigue crack growth under modes I and II are well known, there is a lack of any plausible interpretation in case of a pure mode III crack propagation [1]. Most of experiments allowing mode II and mode III crack propagation were performed in a pure torsion or asymmetrical 4 point bending (e.g. [2-8]). Except for the paper by Nayeb-Hashemi et al. [4], no detailed examinations of the micromechanism of shear mode crack growth were reported in these studies. Therefore, the investigation of shear crack growth mechanisms constitutes a rather big challenge.

A careful fractographical observation of mode II and III growth under pure shear remote loading in the region of very low cycle fatigue were performed by Pokluda et al. [9]. These investigations indicated that the microscopic mode of the pure remote mode II crack extension was rather a mixed I+II mechanism. Similarly, the mode II and the combined mode I+II were dominating microscopical fracture micromechanisms also during the remote mode III loading. The crack growth rate in mode II was found to be about two times higher than that in mode III. As it is shown hereafter, however, the real ratio of the crack tip opening displacements is $CTOD_{II}/CTOD_{III} \approx 0.5$ while the ratio $CTOD_{II}/CTOD_{III} \approx 1$ was presumed in that paper. Therefore, the mode II crack growth rate was, in fact, more than five times higher than the mode III one.

This paper presents a study on the near-threshold crack propagation under shear modes II and III by using two different experimental arrangements and two different steels.

## EXPERIMENTAL ARRANGEMENTS

Two original testing setups (cells) have been designed and utilized in order to assure both pure remote shear modes II and III crack propagation in a single cylindrical specimen. The loading scheme of the first cell is depicted in Fig. 1. The construction of the specimen holder and its orientation with respect to the loading axis provided a pure mode II loading at the "top" and "bottom" sites of the specimen and a pure mode III loading at the "front" and "back" sites. In all other points along the crack front the mixed mode II+III was applied. A circumferential V-notch was machined by a lathe tool at the specimen mid-length and a pre-crack was introduced by a blade mechanism. Finally the specimens were compressed by 20 kN to sharpen the pre-crack (see Fig. 2). Six specimens made of the ferritic steel (< 0.01 %C) with the outer diameter of 8 mm and the inner diameter of 4 mm were loaded by different ranges of the nominal ligament shear stress $\Delta\tau_n$ (the cyclic ratio $R$ = 0.1): 60 MPa (2 specimens), 80 MPa (3 specimens) and 100 MPa (1 specimen). Hereafter, the data obtained on these small specimens are denoted by "S". After the shear mode tests, the specimens were rapidly fractured in the liquid nitrogen. Five specimens made of the austenitic steel X5NiCrTi26-15 were tested by using the shear stress loading range of 180 MPa with the same cyclic ratio. After the tests, the specimens were fractured by a cyclic tensile loading.

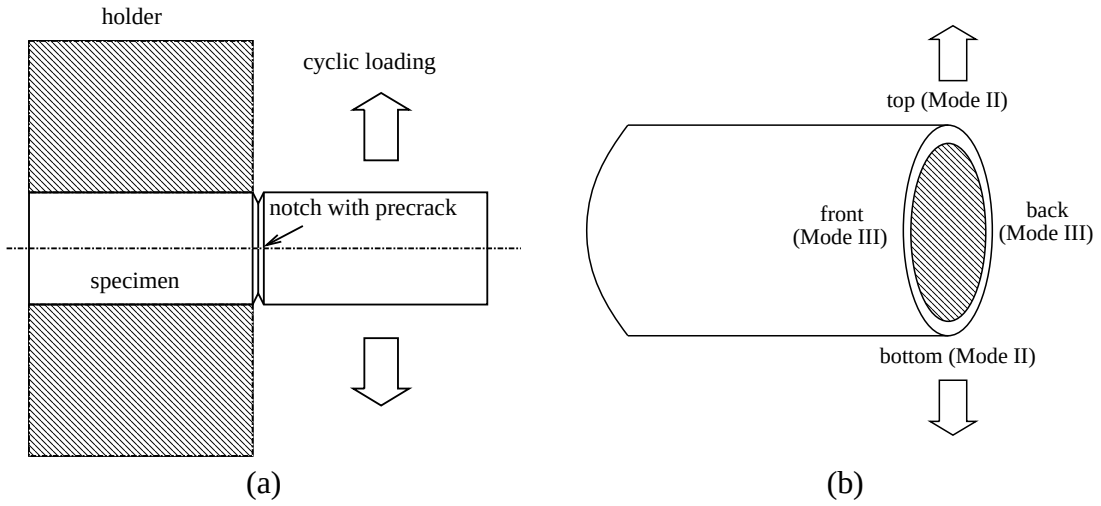


Figure 1. (a) The loading scheme, (b) the loading modes operating at different specimen sites.

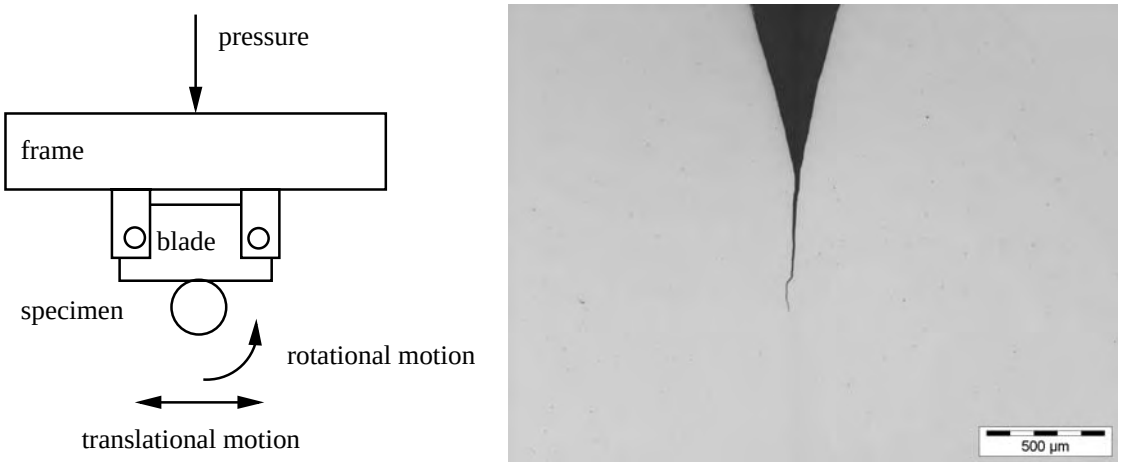


a) b)

Figure 2. (a) The sketch of the pre-cracking procedure, (b) the shape of pre-crack after the compression.

The second special cell for loading specimens made of austenitic steel was manufactured to enable higher loadings (see Fig.3). This cell is an adaptation of the CTS specimen used by Richard et al. for the mixed-mode loading tests (e.g. [10]). The pre-crack was introduced by means of compressive strength of 200 kN. Five specimens with the outer diameter of 25 mm and the inner diameter of 12 mm made of the austenitic steel were tested by using the $\Delta\tau_n$-values of 160 MPa (2 specimens), 200 MPa (2 specimens) and 220 MPa (1 specimen) and the cyclic ratio $R$ = 0.1. Hereafter, the data obtained on these large specimens are denoted by "L". After the shear mode tests, the specimens were fractured by the cyclic tensile loading.

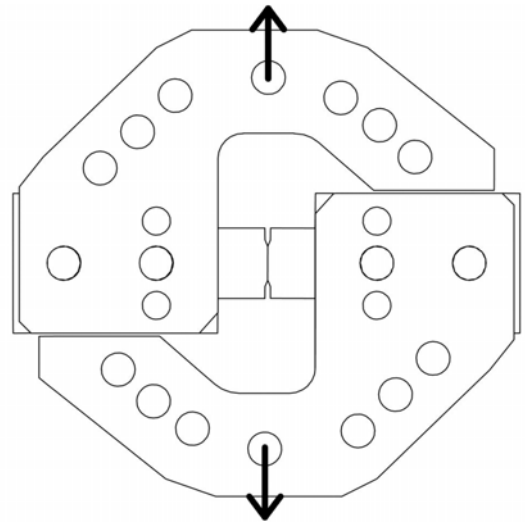

Figure 3. The scheme of the loading cell for austenitic specimens. The loading direction is indicated.

It should be emphasized that, after the production of the notch and the compression loading to form a “ideal pre-crack”, the samples were annealed to avoid a residual stress effect. Both loading cells were constructed as rigid as possible to avoid a static and a cyclic bending of the sample in the crack region.

## THEORETICAL AND EXPERIMENTAL RESULTS

### *Numerical calculation of stress intensity factors*

In order to determine the mode II and mode III stress intensity factors at the crack tip, a numerical analysis was performed by means of the ANSYS code. Although the loaded specimen was modelled as a rotationally symmetric, a full linear-elastic 3D solution had to be used owing to a different symmetry of the loading. In the first step, the stress-strain field along the crack front loaded by the remote shear stress of 180 MPa was determined by utilizing a rough finite-element network. The obtained field was used to a creation of a ring-like submodel with a very fine finite-element network that embraced only the pre-crack region. The submodel surface was loaded by the rim-strain values determined for the same surface in the frame of the rough model. Very precise values of the stress intensity factors $K_{\mathrm{I}}$, $K_{\mathrm{II}}$ and $K_{\mathrm{III}}$ could be calculated in this way. The computations were performed along the circular crack front by applying steps of 3 degrees. A system of local coordinates with one axis oriented in the radial direction was established in each calculation step. Mutual shear displacements of crack flanks were calculated in four points near the crack front.

Table 1. A comparison of numerical and asymptotical solutions obtained for *K*-factors.

| | ANSYS | | Asympt. method |
|---|---|---|---|
| $\tau_{\max}$ [MPa] | $K_{\mathrm{IImax}}$ [MPa.m$^{1/2}$] | $K_{\mathrm{IIImax}}$ [MPa.m$^{1/2}$] | $K_{\mathrm{IIImax}}$ [MPa.m$^{1/2}$] |
| 200 | 3.91 ± 0.60 | 5.36 ± 0.56 | 5.42 |
| 111 | 2.17 ± 0.34 | 2.98 ± 0.36 | 3.01 |
| 89 | 1.74 ± 0.26 | 2.38 ± 0.27 | 2.41 |
| 67 | 1.30 ± 0.17 | 1.79 ± 0.18 | 1.81 |

The values of $K_{\mathrm{I}}$, $K_{\mathrm{II}}$ and $K_{\mathrm{III}}$ were determined by an extrapolation to the crack front. In this way, the values of $\Delta K_{\mathrm{II}}$ and $\Delta K_{\mathrm{III}}$ were determined for all applied nominal shear stress ranges. The ratio of maximal values in pure shear modes II and III was found to be $K_{IIImax}/K_{IImax} = 1.37$ and the values of $K_{Imax}$ were found to be negligible (in two orders lower). As an example, a polar diagram of the maximal values of in the loading cycle $\Delta\tau_n$ = 180 MPa is plotted in Fig. 4. It should be emphasized that the numerical values of $K_{IIImax}$ are in excellent agreement with the asymptotical calculation by means of the asymptotical method [11]. This is documented in Tab. 1, where a comparison of numerical and asymptotical values for different ranges $\Delta\tau_n$ is displayed.

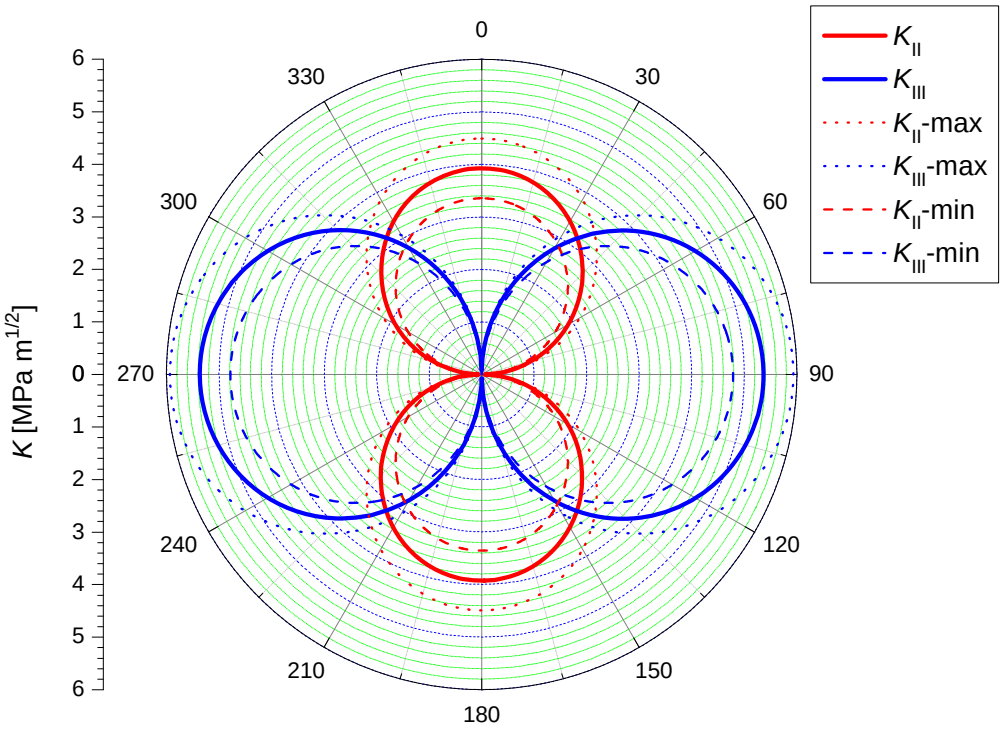


Figure 4. Values of $K_{II}$ and $K_{III}$ along the crack front in angle coordinates.

***Propagation of shear mode cracks***

The spatial shear crack path was determined by the stereophotogrammetrical reconstruction of the fracture surface morphology in the scanning electron microscope. This was performed in selected rectangular regions corresponding to pure mode II and mode III loading of both the austenitic and the ferritic steels.

The fracture morphology of pure mode II and III shear cracks is shown in Fig. 5 for the austenitic steel. The areas corresponding to the pre-crack, the shear crack propagation and the final tensile fracture are marked as well. Practically all the mode II shear cracks were globally inclined from the shear plane in the direction perpendicular on the crack front. This means that the mode II cracks actually propagated under a mixed mode I+II to avoid the retarding friction stress. Such behavior, typical for near threshold region, was previously observed in many cases [1,7,8]. Averaged deflection angles in the direction perpendicular to the crack front were found to be of 47°±16° (austenite) and of 33°±15° (ferrite). The fracture morphology of mode III cracks consisted mostly of factory-roof patterns that are typical for the near threshold region (the small scale yielding). In the case of large yielding, on the other hand, the mode II cracks propagate predominately under local mode II with only a small mode I component and the mode III fracture surfaces are flat without any factory-roof patterns (e.g. [12]). Since the length of the shear mode cracks was an order lower than that of the pre-crack, a nearly constant crack growth rate during the shear propagation could be assumed. Therefore, the crack growth rate was calculated simply by dividing the total

length of shear cracks (the real, not projected) by corresponding numbers of cycles. The near-threshold crack growth curves for both the mode II and the mode III propagation in the austenitic steel are plotted in Fig. 6. Although the experimental data originate from two different sets of specimens (large and small), their mutual link seems to be plausible. The related regression curves follow the Klesnil-Lukas relationship $da/dN = A\left(\Delta K^n - \Delta K_{th}^n\right)$ [13]. The calculated fatigue thresholds $\Delta K_{\mathrm{IIth}}$ = 3.5 MPa·m$^{1/2}$ and $\Delta K_{\mathrm{IIIth}}$ = 4.7 MPa·m$^{1/2}$ are clearly different ($A_{\mathrm{II}} = 1.13\times10^{13}$, $A_{\mathrm{III}} = 2.72\times10^{13}$ [MPa, m]). On the other hand, the exponents are similar ($n_{II}$ = 5.6, $n_{III}$ = 5.1). One can also clearly see that, for the same value of the applied $\Delta K$ range, the crack growth rates for the mode II loading are about 6 times higher than those for the mode III loading. This is in agreement with results achieved in the low-cycle fatigue region [9]. A similar difference was also observed in the case of the ferritic steel in the region very close to the threshold (see Fig. 7). In spite of a large scatter of experimental data (usually observed in that region) the mode III data are systematically shifted to higher $\Delta K$-values. In order to determine the threshold values, however, more experimental data very close to the threshold are obviously needed. These results do not confirm the identity $\Delta K_{\mathrm{IIth}} = \Delta K_{\mathrm{IIIth}}$ as obtained by Murakami et al. [14] for the carbon steel.

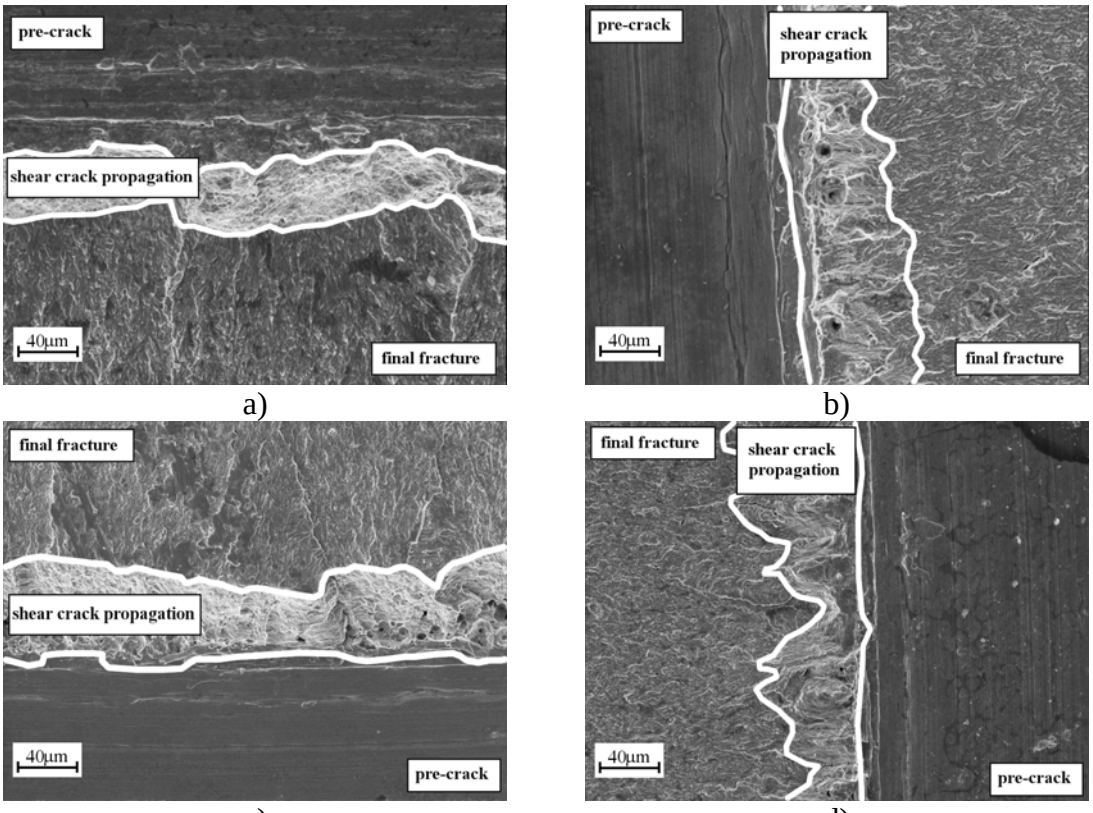

Figure 5. Fracture surfaces of specimens of austenitic steel a) top (mode II), b) front (mode III), c) bottom (mode II), d) back (mode III).

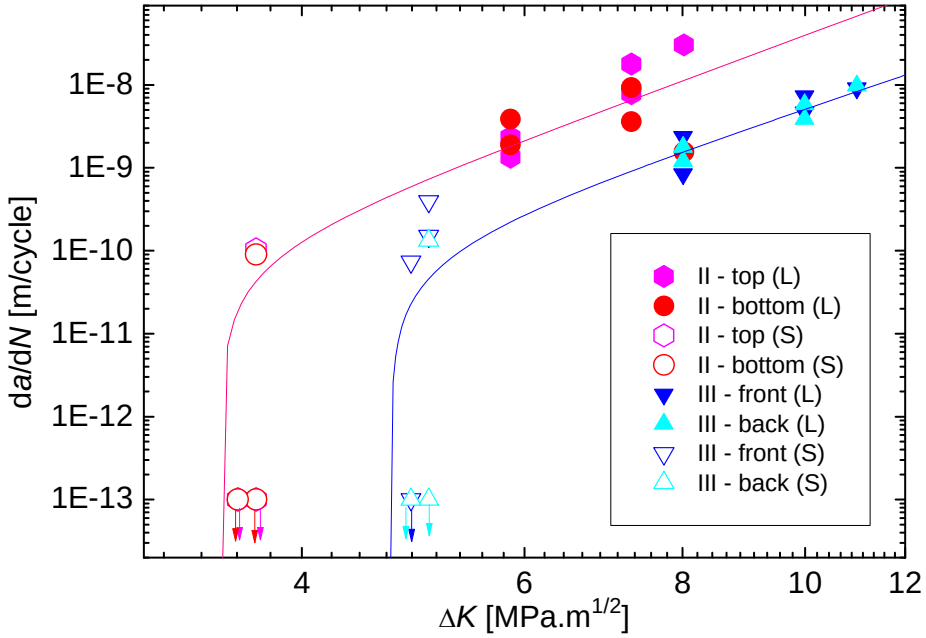


Figure 6. The crack growth curves for the austenitic steel in the near-threshold region.

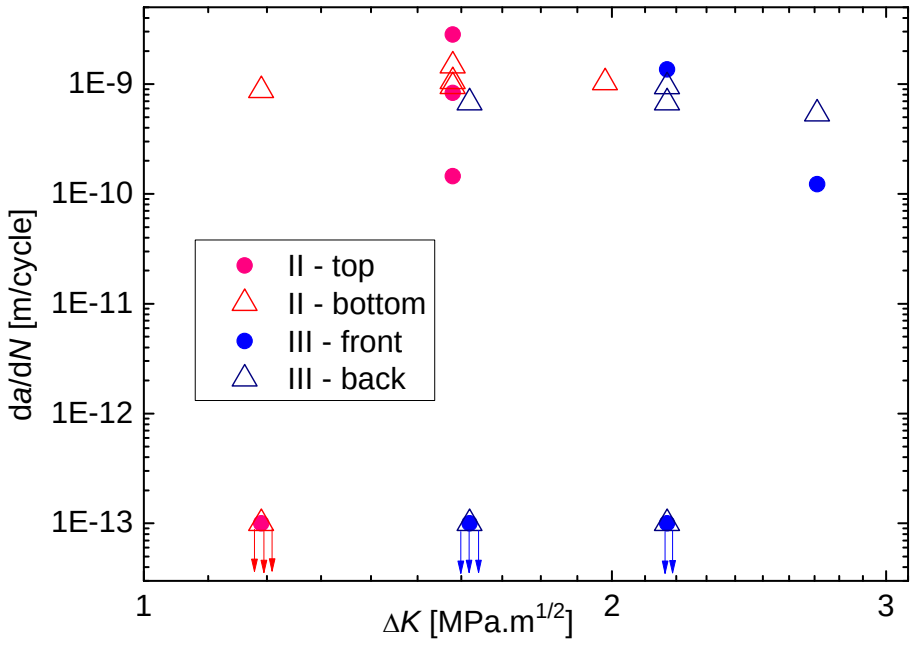


Figure 7. The crack growth data for the ferritic steel close to the fatigue threshold.

The experimental data obtained from the top and bottom sides of specimens do not exhibit a systematic deviation. This confirms that the influence of bending loading can be considered to be negligible.

## CONCLUSIONS

A prototype experiments on the near-threshold crack growth ($R$ = 0.1) enabled a simultaneous mode II and mode III fatigue crack propagation in specimens made of the austenitic and the ferritic steel. The main results of the study can be summarized in the following points:

(i) The FEM analysis of utilized pre-cracked specimens revealed that the ratio of the maximum values of applied stress intensity factors under pure shear modes III and II was $K_{III}/K_{II}$ = 1.37.

(ii) In both steels, the near-threshold crack growth rate under the remote mode II was much higher than that under the remote mode III.

(iii) The threshold values $\Delta K_{IIIth}$ were found to be systematically shifted to higher values in comparison to those of $\Delta K_{IIth}$..

***Acknowledgement***

This research was supported by the Ministry of Education, Youth and Sports of the Czech Republic in the frame of the project MSM 0021630518 and by the Czech Science Foundation (project 106/09/H035).

***References***

1. Pokluda, J., Pippan, R. (2005) *Fat. Fract. Engng. Mater. Struct.* **28**, 179-186.
2. Ritchie, R.O., McClintock, F.A., Nayeb-Hashemi, H. and Rittler, M.A. (1982) *Metall. Trans. A* **13** 101–110.
3. Tschegg, E.K. (1982) *Mater. Sci. Eng.* **A 54** 127–137.
4. Nayeb-Hashemi, H., McClintock, F.A. and Ritchie, R.O. (1983) *Int. J. Fracture* **23** 163–185.
5. Hellier, A.K., Corderoy, D.L.H. and Mc Girr, M.B. (1987) *Int. J. Fatigue* **9**, 95-101.
6. Hellier, A.K., McGirr M.B., Cordero, D.J.H. and Kutajczyk, L.A. (1990) *Int. J. Fracture* **42**, R19-R23.
7. Pook L.P. (2002) *Crack Paths*, Wit Press, London.
8. Murakami Y. (2002) *Metal fatigue: Effects of small defects and nonmetallic inclusions*, Elsevier, Amsterdam – Tokyo.
9. Pokluda, J., Trattnig, G., Martinschitz, C. and Pippan R. (2008) *Int. J. Fatigue* **30**, 1498-1506.
10. Pawliska P., Richard,H.A., Kenning, J. and Diekmann, P. (1991) *Int. J. Fracture* **47**, 43-47.
11. Benthem, JP., Koiter, W.T. (1973) In: *Method of Analysis and Solutions of Crack Problems*, Sih, G.C. (Ed.), Noordhoff International Publishing, Leyden.
12. Vaziri,A., Nayeb-Hashemi, H. (2005) *Engng. Fract. Mechanics* **72**, 617–629.
13. Klesnil, M., Lukas, P. (1980) *Fatigue of Metallic Materials*. Elsevier, Oxford.
14. Murakami, Y., Kusumoto, R. and Takahashi K. (2000) In: *Fracture Mechanics Beyond 2000 (ECF 14)*, Vol. II, Neimitz, A. et al. (Ed.), EMAS, Sheffield.